International Journal of Hydrogen Energy 65 (2024) 337–347

Contents lists available at ScienceDirect

International Journal of Hydrogen Energy

journal homepage: www.elsevier.com/locate/he

Kinetics of iron reduction upon reduction/oxidation cycles

Francesca Cerciello [a,1], Antonio Fabozzi [b,1], Christoph Yannakis [c], Sebastian Schmitt [d], Oğuzhan Narin [d], Viktor Scherer [c], Osvalda Senneca [b,*]

[a] Laboratory of Industrial Chemistry, Ruhr University Bochum, Bochum, 44801, Germany
[b] Istituto di Scienze e Tecnologia per l'Energia e la Mobilità Sostenibili (STEMS)-CNR, 80125, Napoli, Italy
[c] Department of Mechanical Engineering, Ruhr-University, Bochum, Germany
[d] Doosanlentjes, Daniel-Goldbach-Str. 19, 40880, Ratingen, Germany

ARTICLE INFO

Handling Editor: Dr Mehran Rezaei

Keywords:
Iron ore
Hydrogen
Isothermal condition
Non-isothermal condition
Reduction/reoxidation cycles

ABSTRACT

The reduction kinetics of iron ore with H_2 and its re-oxidation with air are investigated by thermogravimetric analysis (TGA) over reiterated reduction/oxidation cycles. Using non-isothermal methods, three steps of reaction have been identified for reduction (activation energies of 133, 30 and 83 kJ/mol) and two for re-oxidation (30 and 70 kJ/mol). Isothermal analysis, instead, leads to wrong kinetic expressions. A remarkable "annealing" effect is observed: when the temperature of reduction is increased from 600 to 850°, the pre-exponential factors of the re-oxidation step decrease by an order of magnitude. Upon repeated cycles, reactivity decreases in the first three cycles, but is restored after 4–5 cycles and even increases upon further cycles. X-ray Diffraction (XRD) analysis shows changes in the crystalline phase of hematite upon reduction and re-oxidation, suggesting a possible spin-flip effect. After 4–5 reiterated cycles the opening up of porosity may counterbalance negative changes at the nanoscale.

1. Introduction

On Earth, iron mainly appears in the form of its oxides; furthermore, hydroxides, carbonates and sulfides are also common [1]. However, the two most important oxides are hematite (Fe_2O_3) and magnetite (Fe_3O_4) [2]. In the last decade, iron oxide reduction has been widely investigated for carbon dioxide (CO_2) capture and abatement in chemical-looping combustion [3,4]. However, in order to obtain metallic iron, the iron oxide has to be reduced from the trivalent (or divalent) state to the metallic one [5]. For this reason, a reducing agent is required which must have a higher affinity to oxygen than the iron itself, under given process conditions [6]. Currently, iron ore reduction is mainly based on carbon as an energy source and reducing agent, but hydrogen can also be employed as an effective reduction agent [7]. Nevertheless, the kinetic analysis of reduction results complex because it is a two-step mechanism below 570 °C and a three-step mechanism above 570 °C. If the temperature is below 570 °C, the reduction to Fe occurs from Fe_2O_3 to Fe_3O_4 and continues to Fe [8]. The intermediate oxide named wüstite, $Fe_{(1-y)}O$, is not stable at temperatures <570 °C, while at reduction temperatures >570 °C, $Fe_{(1-y)}O$ must also be considered in the reduction process [9]. In this case, the reduction occurs from Fe_2O_3 *via* Fe_3O_4 to $Fe_{(1-y)}O$ and continues afterward to Fe [10]. Beyond temperature, pressure, and gas composition, the properties of the material that should be reduced, such as grain size, morphology and porosity, affect the reduction advancement [11] (see Scheme 1).

A wide set of papers reported in the literature addressed the kinetics of iron reduction and oxidation [12–14]; however, a variety of discrepancies, reported in more detail in section 4 of the paper, can be observed in the kinetic parameters, such as the activation energy, related to the reduction of iron oxide by hydrogen [15].

During the reduction and oxidation processes of iron ores in a reactor, severe changes in their structure occur [16]. In the early stages of heat treatment and reduction, transformations at both the chemical and structural levels are obtained [17]. Structural annealing has been reported to affect the reaction rate especially in the final reduction stages [18]. Notably, reiterated cycles can produce additional changes in the microstructure and consequently in the iron ore reactivity [19].

Recently, reduction/oxidation cycles of iron oxides have been addressed in the literature for chemical looping [20,21]. Jeong et al. developed a prototype composed of Fe/TiO_2 as a catalytic system for a

* Corresponding author.
E-mail address: osvalda.senneca@stems.cnr.it (O. Senneca).
[1] F.C. and A.F. equally contributed to this work.

https://doi.org/10.1016/j.ijhydene.2024.04.008
Received 22 December 2023; Received in revised form 26 March 2024; Accepted 1 April 2024
Available online 7 April 2024

chemical looping *via* stepwise ethane dehydrogenation, reduction T < 550 °C, with a CO_2 activation to CO during the oxidation, T > 700 °C, to gain a higher yield than the conventional dehydrogenation of ethane by co-feeding CO_2, after five reduction/oxidation cycles [22]. Furthermore, iron oxides have been employed in a reduction/oxidation cycle as carbon-free carriers of renewable energy [23]. Specifically, De Biagi et al. reported on a reduction/oxidation process for energy conversion, where iron is used as a fuel [24] to sustain high-temperature oxidation. The advantage of using iron, as fuel is that it produces no CO_2 emissions, and that, after combustion, iron oxides can be easily recovered stored and transported to reduction facilities. Subsequently, the iron oxide can be reduced by the Midrex process [25], or in ironmaking [26], or *via* the redox process [27].

Nevertheless, although great efforts have been made based on the investigation of all parameters that influence the reduction and the oxidation of the iron ores, comprehensive kinetic models inclusive of changes of microstructure and porosity, especially upon reiterated reduction/oxidation cycles, are still missing. This has instead been done in combustion and gasification of solid carbonaceous fuels, where progressive loss of reactivity due to thermal annealing of the structure has been included in advanced kinetic models [28].

The first part of the present work aims at obtaining kinetics expressions for reduction of "fresh" iron with H_2. This entailed an extensive campaign of thermogravimetric (TGA) experiments with an iron ore powder at temperatures up to 850 °C and H_2 concentrations up to 32mol %. Different kinetic analysis methods were applied, and results were compared with literature data.

In the second part of the work, re-oxidation of the iron samples was investigated. To this end, the iron ore powder was firstly reduced with H_2 and then re-oxidized with air in the TGA. The reduction step was carried out at different temperatures and with different H_2 concentration in order to assess the effects of the severity of the precedent reduction stage on the kinetics of re-oxidation.

In a third part of the work, repeated cycles of reduction with hydrogen and re-oxidation with air have been carried out and the progressive changes in samples reactivity have been measured, in order to test the performance of the material in looping processes.

Changes in iron ore microstructure were investigated by X-ray Diffraction (XRD) and Scanning Electron Microscope (SEM) analysis, in order to compare the reactivity changes induced by reduction and re-oxidation on particles morphology and microstructure. Although further work is certainly needed to fully characterize the structural changes over repeated cycles of operation, the present work represents a first step towards the development of kinetic models suitable for reduction/oxidation cycles in the framework of the fast-growing field of iron ore-based science and technology.

2. Materials and methods

South African Iron Ore Khumani (IOK) provided by laboratory of industrial chemistry, Ruhr University Bochum (RUB), has been investigated.

The qualitative analysis in order to identify metal components was carried out by means of X-Ray Fluorescence (XRF), using a Nexde-Rigaku instrument.

Notably, IOK is a natural iron ore and contains few percentages of Si, Al, and only traces of other components, as can be appreciated from the results of XRF, reported in Table 1. The contribution of mineral impurities, such as Ca and Mg, which are most impactful on the reactivity of iron ores [8,29] with H_2, is therefore expected to be modest.

The IOK sample had a nominal particle size of 90–200 μm, however, laser granulometry detected also the presence of a relevant fraction (40% by volume) of particles with size in the order of 10 μm (Fig. S1 in Supplementary material). The fine particle size was selected to perform kinetic measurements under kinetic controlled conditions.

The reduction/oxidation experimental campaign included the following measures and tests:

i) reduction in TGA-DSC under non-isothermal (heating rates between 2 and 20 °C/min) and isothermal conditions (temperatures between 500 and 850°) with H_2 concentration in the range 5–30 mol%. Experimental data sets are summarized in Table S1;
ii) oxidation in TGA-DSC under non-isothermal (heating rates between 2 and 20 °C/min) and isothermal conditions (temperatures between 500 and 850°) in air. Experimental data sets are summarized in Table S1;
iii) reduction/oxidation cycles in TGA-DSC, summarized in Table S2.

Tests have been carried out in a Netzsch 409 TG-DSC (Differential Scanning Calorimetry) apparatus. In each test, approximately 20 mg of sample has been loaded in an alumina crucible and heated up in a gas flow of 200–300 ml/min of desired composition, according to the heating program reported in Tables S1 and S2. Notably, between any reduction and oxidation step and vice versa the sample was held in inert flow. The value of H_2 concentration in the reduction tests has been

Table 1
XRF analysis of IOK.

Elements	Area %
Fe	89.9
Si	5.1
Al	2.7
K	0.45
Mg	0.45
Mn	0.25
Ti	0.2
Cl	0.18
P	0.15
Ca	0.13
S	0.07
Cr	0.06
Ni	0.05
Ba	0.05
Sn	0.04
Sr	0.04
V	0.03
Zn	0.03
Te	0.02
Zr	0.01
Ce	0.01

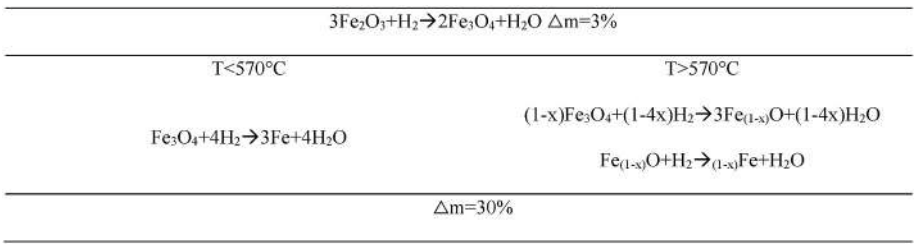

Scheme 1. Reduction reaction scheme.

checked by ABB analysers connected at the TGA outlet. The mass loss recorded during the test has been worked out to calculate:

- the final fractional mass loss $\frac{m_0-m_f}{m_0}$ and mass gain $\frac{m_f-m_0}{m_0}$ during reduction/oxidation (where m_0 and m_f are the mass at the beginning and at the end of the reduction or oxidation test);
- DTG curves of derivative mass loss $\frac{1}{m_0}\frac{dm}{dt}$ versus temperature;
- instantaneous reaction rate curves of dx/dt versus x, with conversion x defined as $x = \frac{m_0-m}{m_0-m_f}$;
- the heat of reaction of reduction/oxidation from the integral of DSC curves registered during the test.

A kinetic analysis of reduction and oxidation has been carried using both isothermal and non-isothermal TGA results. Non-isothermal TGA data have been worked to obtain Arrhenius plots of $\ln\left(\frac{dx}{dt}\frac{1}{1-x}\right)$ versus 1/T. For isothermal tests, instead, Arrhenius plots have been based on reaction rate averaged over the first 50% of conversion ($R_{av} = \frac{0.5}{t0.5}$, where $t_{0.5}$ is the time required to reach 50% of conversion).

SEM (Scanning Electron Microscopy) analysis of reduced and oxidized samples for has been performed by SEM FEI Ispect S, Column E-SEM W, Source: 200 V–30 KV, filament: tungsten equipped with an Everhart–Thornley detector (ETD).

The crystallinity of IOK as received, IOK treated with H_2 and re-oxidized structures was investigated by an X-Ray powder Diffraction (XRD) analysis in the 2Θ range 3–90° using a Rigaku Miniflex 600 automated diffractometer equipped with a CuKα radiation source. Phases were identified by using the PDF-5+ 2024 database (ICDD International Centre for Diffraction Data®, Newtown Square, PA, USA) and the Rigaku Smart Lab II software v4.5.162.0. The determination of Indices Refraction Ratio (RIR) was performed without considering the amorphous phase.

3. Results and discussion

3.1. Reduction tests

Initially, reduction tests from Fe_2O_3 with H_2 were carried out. The final mass loss obtained in the reduction tests was 28–30%, which is consistent with the following reaction scheme, which, for a 100% pure Fe_2O_3 would imply a mass loss of 33%:

Notably, two or three stages of reaction are expected: two at T < 570 °C and three at T > 570 °C. This is indeed consistent with reduction patterns observed under both isothermal and non-isothermal tests, summarized in the following. Fig. 1a reports a typical DTG curve (derivative of the weight loss versus temperature) obtained at the heating rate of 5 °C/min with 6% H_2. In particular, three peaks in the temperature ranges: 350–500 °C; 500–700 °C; 700–850 °C are detected. Examples of curves of instantaneous reaction rate (dx/dt) versus conversion (x) are shown in Fig. 1b.

Particularly, in isothermal tests at temperature above 600 °C a fast reaction stage is observed at conversion below 10%, followed by two other stages between x = 20–30% and at x = 40% respectively. The first two stages partly overlap while the last stage is the most remarkable and best resolved.

At the reduction temperature of 550 °C, the peak in reaction rate at conversion below 10% is still detected followed by only one slow stage of reaction with a maximum around x = 30%. Furthermore, the instantaneous reaction rate of the first fast reaction stage ($R_{max\ 1}$), and the time $t_{0.5}$ and $t_{0.8}$ required to reach 50% and 80% of conversion are reported in Table 2 for the different reduction conditions tested.

3.2. Re-oxidation tests

Results of the oxidation tests carried out in air on a set of samples, which had been previously reduced at different temperature and with different H_2 concentration, are summarized in Fig. 2 and Table 3. The final mass gain obtained in the oxidation tests varied in the range 25–40 % (relative to the weight of the reduced sample) as can be observed from TG curves.

DTG curves acquired upon non-isothermal oxidation of samples that have been pre-reduced under different conditions of temperature and hydrogen concentration are shown in Fig. 3.

Notably, the peaks of the DTG curves shift towards higher temperatures as the severity of the temperature of reduction pretreatment increases, suggesting a negative effect of temperature on the re-oxidation rate, i.e. an "annealing" effect can be observed based on the severity of the conditions of reduction. The most reactive sample is the one reduced

Table 2
Reduction rate and timescale.

T,°C	H_2	$R_{max\ 1}$	$t_{0.5}$, min	$t_{0.8}$ min
500	6%	0.011	96	176
550	6%	0.016	83	148
600	6%	0.015	57	99
650	6%	0.022	47	76
700	6%	0.035	46	88
750	6%	0.036	38	63
850	6%	0.055	21	38
500	16%	0.025	35	63
650	16%	0.044	19	31.5
750	16%	0.08	12	20
500	32%	0.038	15	27
650	32%	0.145	8.5	14.75
750	32%	0.17	5.5	8.9
850	32%	0.2	4	6.5

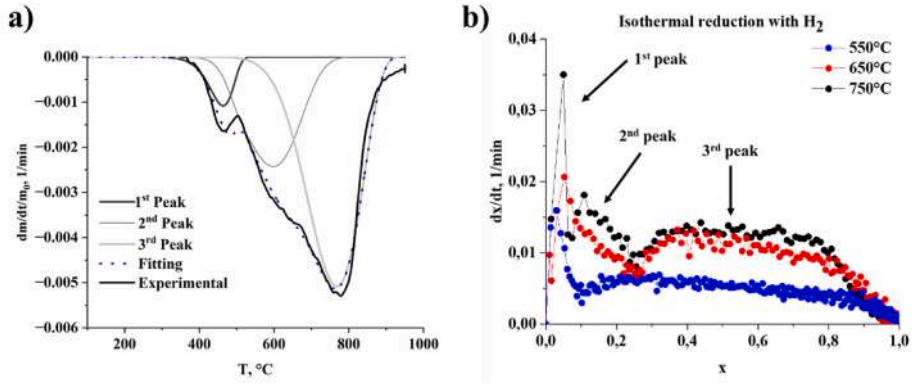

Fig. 1. a) DTG curve for reduction of iron ore at 5 °C/min with 6% H_2 (experimental and kinetic model results); b) Examples of curves of instantaneous reaction rate versus conversion in isothermal tests.

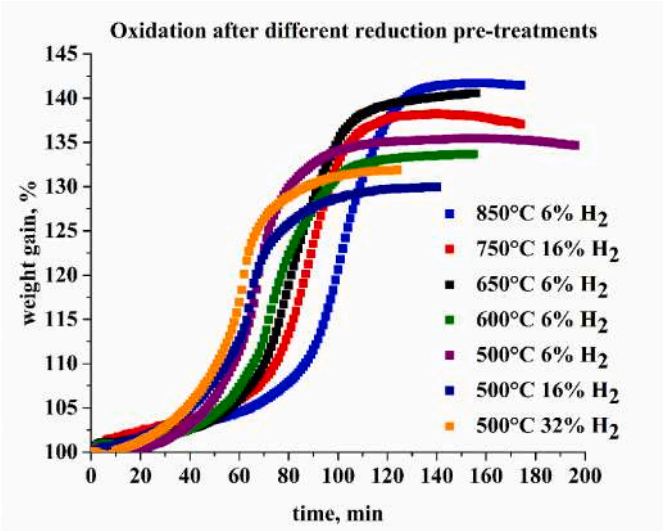

Fig. 2. TG curves of non-isothermal oxidation in air for samples previously reduced with different temperature and H_2.

Table 3
Weight gain and DTG peaks of re-oxidation.

T,°C	H_2	DTG_{max}	Mass gain%
500	6%	360	35
500	16%	365	29
500	32%	350	31
600	6%	385	34
650	6%	425	41
750	16%	475	38
850	6%	540	41

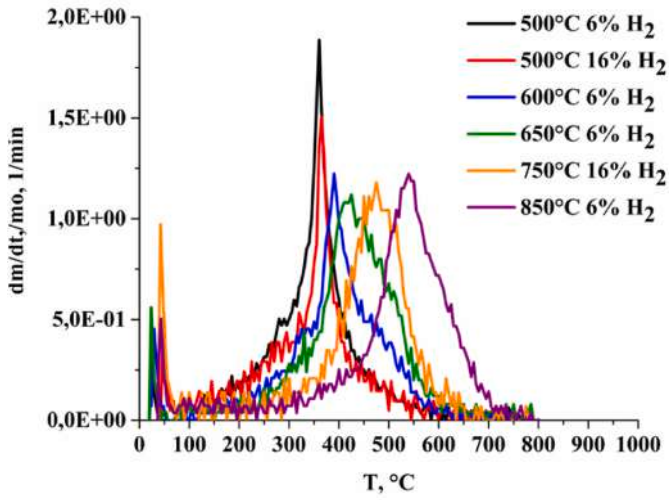

Fig. 3. DTG curves of non-isothermal oxidation in air for samples previously reduced with different temperature and H_2.

at 500 °C with 32% H_2. The least reactive the one reduced at 850 °C with 6% H_2.

The "annealing" effect upon reduction-oxidation steps may be related to structural changes that affects reaction rate. This will be discussed later, in the paragraph on morphological and microstructural analysis.

3.3. Reduction-oxidation cycles

The results of sequences of reduction/oxidation carried out under condition described in Table S2 and are summarized in Table 4 and Figs. 4–5. Fig. 4 reports the TG curve over a reduction-oxidation sequence at 650 °C (with 16% H_2 in the reduction step and air in the oxidation step). Notably, the steps have been prolonged in order to reach a steady sample weight. It can be noted that the time for reduction and the time for oxidation under such conditions of temperature and gaseous atmosphere are comparable and in the order of 30 min.

In cycles of oxidation and desorption with multiple iterations (5–6) at 650 °C (with 16% H_2) and 750 °C (with 30% H_2) the duration of the steps has been fixed at 20 and 10 min, respectively. The results in terms of mass loss and gain at each cycle are reported in Table 4.

It can be observed that the mass loss/gain was not the same for all steps, ranging between 55 and 85%. In fact, a minimum is observed in the second-third stage, showing that the performance of the iron ore initially decreases in the early cycles but improves after, as shown in Fig. 5a.

The sample after 6 cycles at 650 °C has been subjected to standard isothermal TGA reduction run at 650 °C with 16% H_2 and results have been compared with those of a similar reduction test carried out on the fresh iron ore. As shown in Fig. 5b, the reactivity of the iron ore after multiple reduction-oxidation cycles has approximately doubled.

3.4. Microstructural and morphological investigation of iron ore

Microstructural and morphological investigation of samples subject to different reduction and re-oxidation treatments has been performed by XRD and SEM.

Fig. 6 reports the results of the structural investigation carried out by XRD on raw IOK (black), IOK treated with 6% H_2 at 850 °C (blue) and then re-oxidized in air (red).

The XRD pattern of the IOK shows diffraction peaks (labelled as 1 in Fig. 6) corresponding to crystalline phases of the hematite, with a minor diffraction peak attributable to the SiO_2 (labelled as 2). Indeed, from the Indices Refraction Ratio (RIR), which is expressed in wt%, the IOK XRD pattern results to be composed for 89% of hematite and 11% of the SiO_2, which is in relatively good agreement with the qualitative results of XRF analyses, in consideration also of the fact that the hematite content is underestimated with the RIR method because of the likely presence of an amorphous hematite phase. When IOK is more extensively reduced to obtain metallic iron (treatment with H_2 at 850 °C), the XRD pattern shows the typical peaks of the α-Fe (labelled as 3) with a RIR of 97 % and only 3% of SiO_2 (labelled 2). When the sample is further on re-oxidized, in the XRD pattern hematite is again detected, with a RIR of ~93%, and SiO_2 with a RIR of ~7%, but the hematite crystalline phases (labelled as 4) is different from the one present in starting material (labelled as 1). It is likely that after reduction all the iron present, even the fraction, which was originally amorphous, rearranges into crystalline hematite. It could be speculated that the first-order magnetic transition, named the Morin transition, occurs. This transition has indeed been reported by Hu et al. (Fe_2O_3 Card Number: 01-073-3825) [30] to occur beyond the Néel

Table 4
Mass loss and mass gain throughout reiterated reduction/oxidation cycles.

Cycle	Temperature			
	650 °C		750 °C	
	Reduction	Oxidation	Reduction	Oxidation
	20 min	20 min	10 min	10 min
	16% H_2	air	32% H_2	20% O_2 in Ar
1	−18.6%	13%	−22.4%	22.65%
2	nd	nd	−20.5%	20.06%
3	−16.0%	18%	−18.6%	21.6%
4	−17.9%	19.7%	−20.9%	24.9%
5	−19%	19.5%	−21.6%	21.6%
6	−19.5%	19.5%	−24%	24%

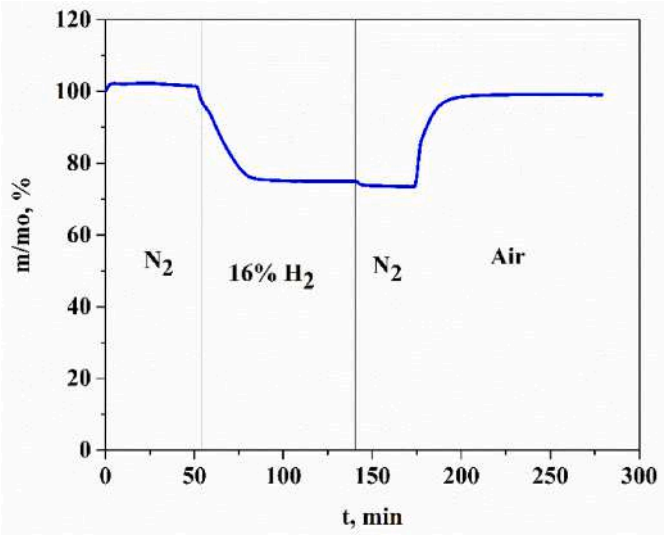

Fig. 4. TG curve during isothermal reduction-oxidation at 650 °C.

Temperature of 680 °C. In particular, below the Morin transition, antiferromagnetic order is detected, while above the Morin transition a spin-flip transition, due to development of antiferromagnetic order in the basal plane of the crystal, with a ferromagnetic contribution, occurs.

Selected SEM micrographs of IOK after isothermal TGA reduction with 6% H_2 at different temperature are reported in Fig. 7.

Particles reduced at 600 °C appear edgy and with rather smooth surface. Porosity in these particles seems negligible. Increasing the temperature of reduction from 600 to 750 °C and 850 °C a variation of the particles surface from smooth to rough is detected. The contour of the particles becomes, indeed, less edgy and at higher magnification longitudinal cricks become evident.

The morphological changes occurring upon reduction at 750 °C with 16% of H_2 are shown in Fig. 8. From comparison with Fig. 7, it can be observed that increasing the H_2 percentage from 6 to 16%, while keeping the reduction temperature fixed, results in further increase of particles surface roughness and porosity.

Fig. 8 reports the SEM pictures of IOK sample, which has been reduced at 750 °C with 16% H_2 and then re-oxidized in air at 10 °C/min up to 850 °C. Some couples of particles seem to be attached at one extreme (highlighted in the red circle), suggesting incipient, but still very limited aggregation. However, at this stage, swelling appears to be negligible and the original overall surface/volume ratio of the particles is relatively preserved.

Finally, Fig. 9 shows SEM images of a sample, which has undergone 6 cycles of reduction (with 16% of H_2) and oxidation (with air) at 750 °C.

It can be noticed that upon six cycles of reduction/oxidation steps much more remarkable changes in particles morphology occur:

a) millimetric size agglomerates of small particles are formed; b) needle-like-filamentous material appears on the particles surface; c) extensive development of porosity is observed with formation of a sponge like microstructure. Even though accurate measurement of the porosity by gas adsorption or mercury intrusion has not been carried out in the present work, image analysis of the SEM pictures was used to obtain a rough estimate of pore sizes. Pores turned out to have diameters between 25 and 250 nm.

The results on microstructural changes, even though not exhaustive, can provide some clues on the origin of the annealing effect observed upon reduction-oxidation steps. As expected from the literature, significant and steady changes of the structure occur already upon the first reduction step (at T = 750 °C) [31]. In terms of porosity, cracks are formed at this stage, which open up the porosity, however, it must be remarked that this effect should increase the reactivity and can by no

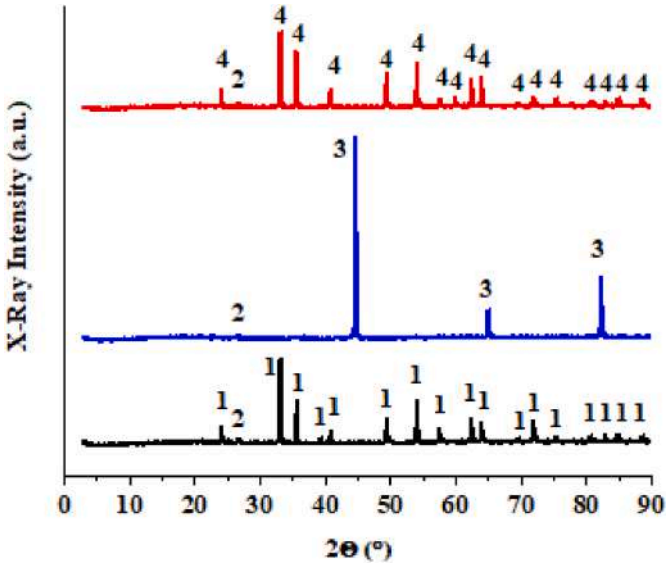

Fig. 6. XRD diffractograms of IOK (black), IOK reduced at 850°Cwith 6%H_2 (blue) and re-oxidated at 850 °C with the air (red). The crystalline phases, with ICDD codes, are indicated: 1 = IOK, Fe_2O_3, 01-089-0597; 2 = SiO_2, 01-082-0511; 3 = α-Fe, 01-080-3816; 4 = Hematite, Fe_2O_3, 01-073-3825. (For interpretation of the references to colour in this figure legend, the reader is referred to the Web version of this article.)

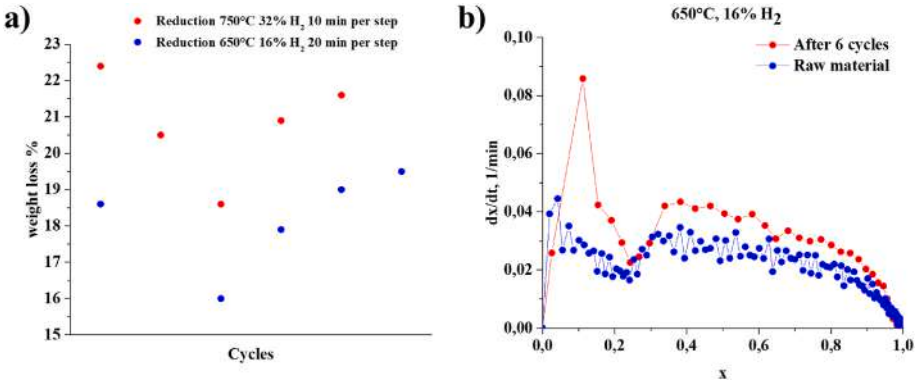

Fig. 5. a) Mass loss attained at each reduction step throughout reiterated cycles; b) Curves of instantaneous reaction rate (dx/dt) versus conversion for fresh iron ore and sample after 6 reduction/oxidation cycles at 650 °C.

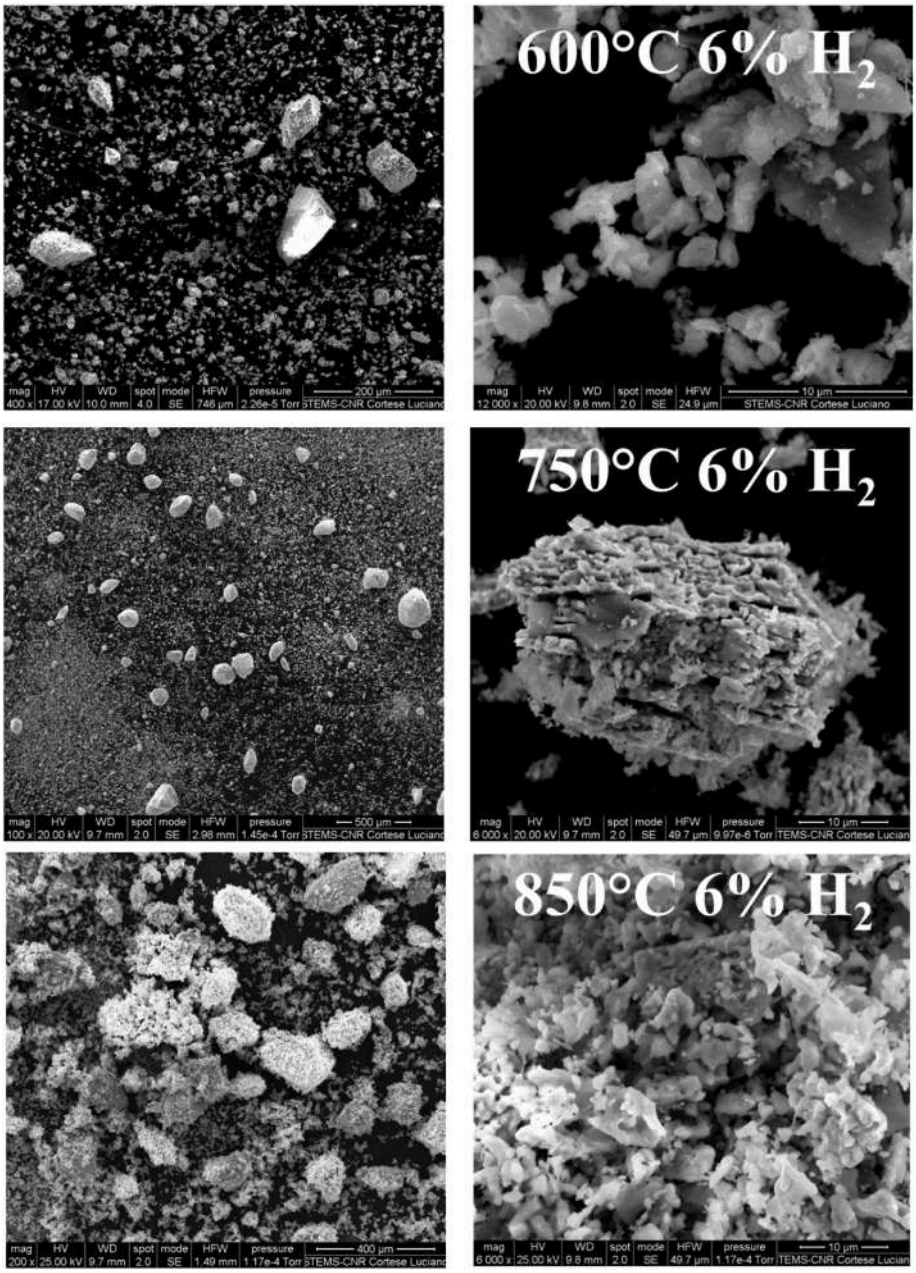

Fig. 7. SEM images of IOK after isothermal TGA reduction at different temperatures with 6% H_2.

means considered responsible for annealing. A negative effect on the materials reactivity could be expected, instead, from sintering phenomena, but these appear to be modest after a single reduction step consistently with the fact that sintering is reported to be relevant at temperatures (950 °C) [31] higher than those investigated in the present work. Another important effect, that could come into play, is the re-distribution of contaminants. Indeed, the accumulation of certain gangue elements at the metal/oxide interface has been reported to affect the reduction kinetics of iron by Ref. [32], as well as sintering [31]. However, XRD and XRF, showed that the main impurity in IOK is SiO_2, while Ca and Mg, which are probably the most impactful impurities [33], are present only in trace. Altogether, the most intriguing microstructural changes observed in the present work can be considered the spin-flip effect suggested by XRD; however, its implication on samples reactivity and annealing is to be further investigated.

4. Kinetic analysis

It has been mentioned in the introduction that reduction of iron by H_2 implies different reaction steps and that the kinetic parameters reported in the literature are highly scattered. Thermogravimetric analysis (TGA) has been widely used for kinetic studies. TGA campaigns can be based on isothermal experiments (I-TGA) at different temperature and on non-isothermal experiments (NI-TGA), where the temperature is raised at different constant heating rates. The most popular software packages for kinetic analysis rely on multiple NI tests and apply the methods of Kissinger [34], Friedman [35], Kissinger–Akahira–Sunrose [36], Flynn–Wall–Ozawa [37], Coats–Redfern [38], Starink [39]. However, it must be remarked that these methods produce meaningful results only under the following hypothesis:

A. Inter- and intra-particle mass and temperature diffusion resistances are negligible.

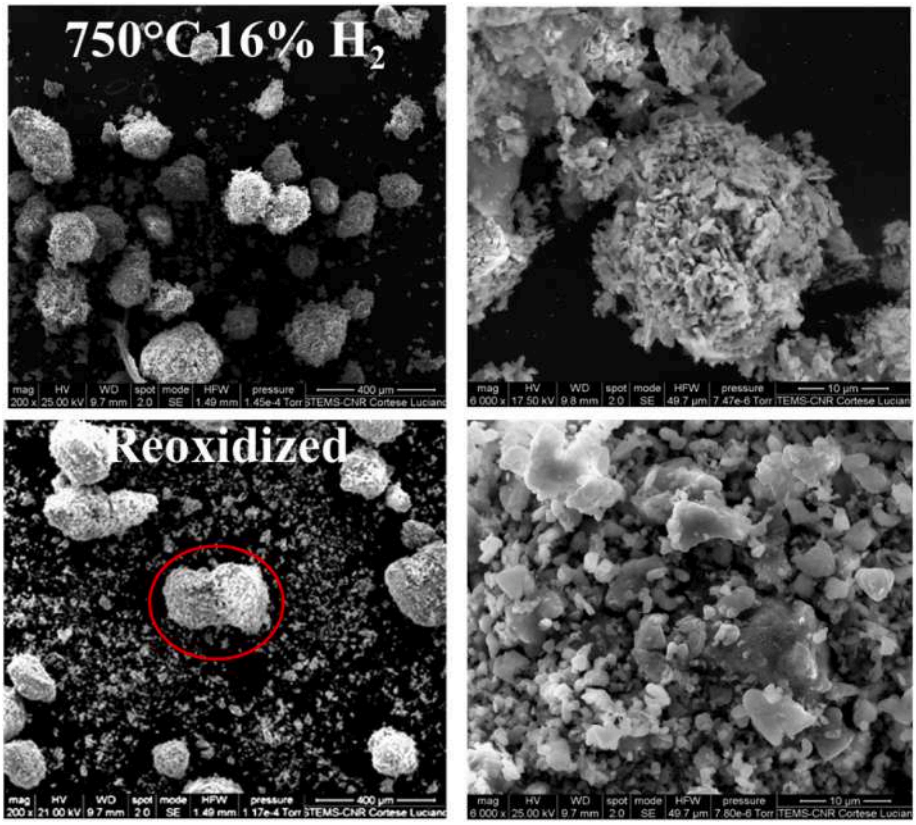

Fig. 8. SEM images of IOK after isothermal TGA reduction at 750 °C with 16% H_2 and non-isothermal re-oxidation in air up to 850 °C.

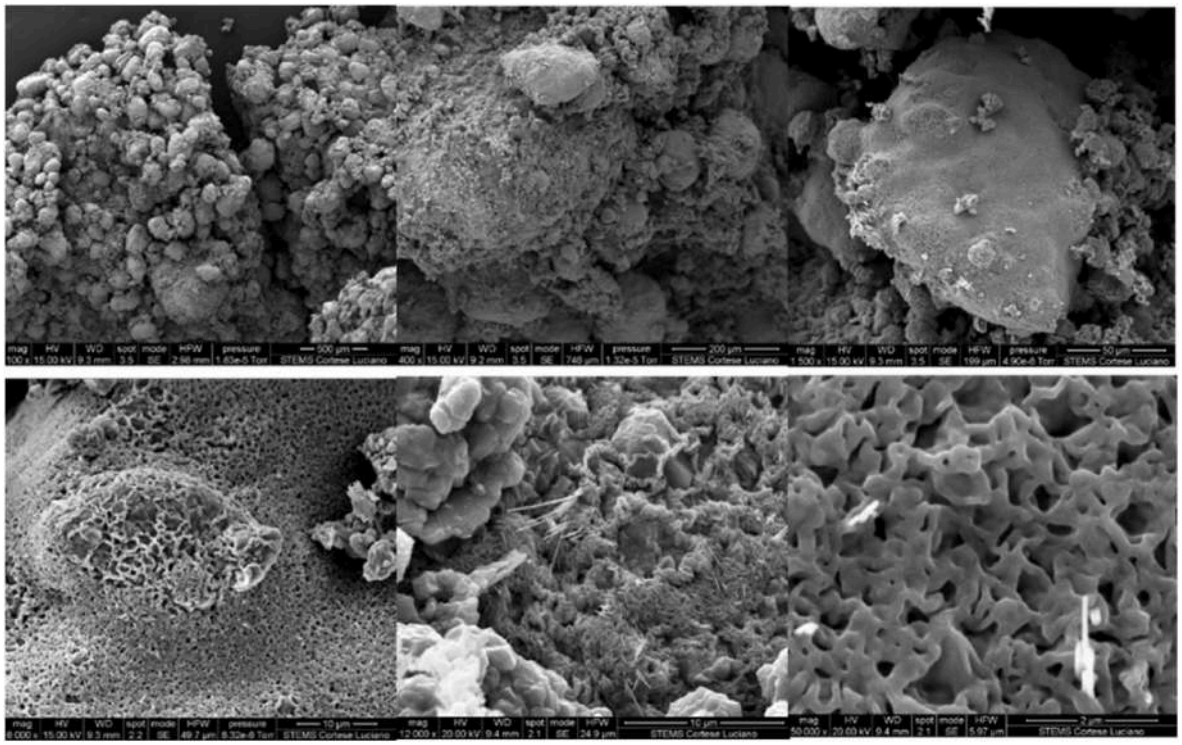

Fig. 9. SEM images of IOK after 6 cycles of isothermal TGA reduction at 750 °C with 16% H_2 and re-oxidation at 750 °C with air.

Table 5
Reduction of iron oxides by hydrogen with their amounts of apparent activation energy.

Operative conditions	Reduction Reaction	E_a (kJ/mol)	References
Non-Isothermal with H_2	$Fe_2O_3 \rightarrow Fe_3O_4$	246	[40]
	$Fe_3O_4 \rightarrow Fe$	93.2	
	$Fe_2O_3 \rightarrow Fe_3O_4$	162.1	
	$Fe_3O_4 \rightarrow Fe$	103.6	
	$Fe_2O_3 \rightarrow Fe_3O_4$	139.2	[41]
	$Fe_3O_4 \rightarrow FeO$	77.3	
	$FeO \rightarrow Fe$	85.7	
	$Fe_2O_3 \rightarrow Fe_3O_4$	89.1	[42]
	$Fe_3O_4 \rightarrow Fe$	70.4	
	$FeO \rightarrow Fe$	104.0	[43]
Isothermal with H_2	$Fe_2O_3 \rightarrow Fe$	57.1	[44]
	$Fe_2O_3 \rightarrow Fe$	72.7	
	$Fe_2O_3 \rightarrow Fe$	89.9	
	$Fe_2O_3 \rightarrow Fe_3O_4$	30.1	[45]
	$Fe_2O_3 \rightarrow FeO$	47.0	[46]
	$FeO \rightarrow Fe$	30.0	
	$Fe_2O_3 \rightarrow Fe$	47.2	[47]
	$Fe_2O_3 \rightarrow Fe$	51.5	
	$Fe_2O_3 \rightarrow FeO$	42.0	[48]
	$FeO \rightarrow Fe$	55.0	
	$Fe_2O_3 \rightarrow FeO$	33.0	[7]
	$FeO \rightarrow Fe$	11.0	

B. Reactions result in a single stage of mass loss or in well-resolved and defined sequential stages.
C. The structure of the solid reactant is relatively constant throughout the experiment.

If any of these conditions are not fulfilled, routine kinetic analysis from TGA results can lead to severe errors and an expert-case sensitive approach must be developed in order to gain insightful results.

It is evident that, due to the complexity of its reaction scheme, reduction of iron by hydrogen does not fulfil the conditions under which TGA provides easy and reliable kinetic parameters. Another problem is the formation of non-porous product layers around the particles, especially for larger particles sizes, which can lead to rate limitation by solid-state diffusion. On top of this, the structure of the solid reactant cannot be assumed constant throughout the experiment, because obviously the reduction of iron oxides leads to different metallic iron formations (hematite, magnetite, wüstite). It is also possible, especially for relatively large particles, that the different reactions occur simultaneously within the same particles at different radial locations, thus making it difficult to distinguish and resolve reactive events. These problems may be the reason why very controversial results have been reported in the literature on the kinetic parameters, with activation energy values varying by order of magnitude (Table 5).

In the present work, a small size cut has been selected (90–200 μm) to avoid internal and external mass transfer limitations. Calculations of the Biot and Thiele numbers, reported in Supplementary material, validate this assumption.

Table 6
Reduction kinetics from NI-TGA Arrhenius plots.

T [°C]	E_a [kJ/mol]	k_o [1/(min·atm)]
<550	133	3E+08
550–700	33	17
>700	83	6700

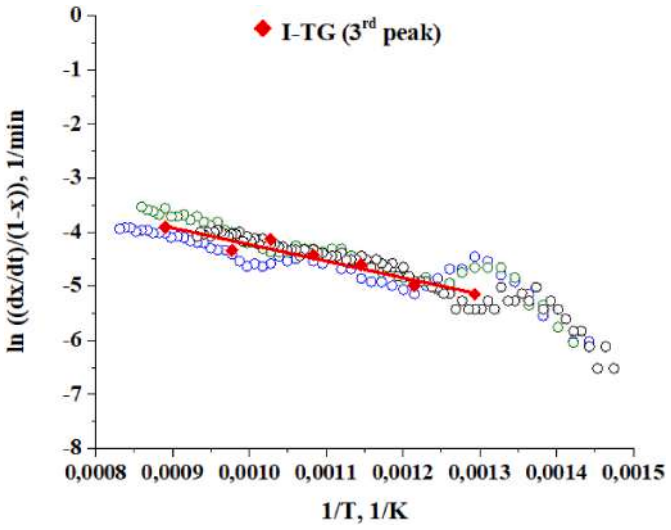

Fig. 11. Iron ore reduction kinetics with 6% H_2. I-TGA at different temperature overlaid to NI-TGA at different heating rates.

Different strategies have been followed to obtain the kinetic rate expressions of iron ore reduction from the TGA campaigns.

The experimental results reported in previous paragraphs (compare Fig. 1) showed that in non-isothermal tests of iron reduction three stages of reaction can be distinguished, whereas in isothermal tests, two to three stages of weight loss are registered, depending on the temperature of reaction.

Arrhenius plots have been calculated for NI-tests at different heating rates for the first and third peak of the isothermal tests (the second peak was not always clearly distinguishable), assuming a simple kinetic law, of the type:

$$\frac{dx}{dt} = k_o p_g \exp^{-\frac{E}{RT}}(1-x)$$

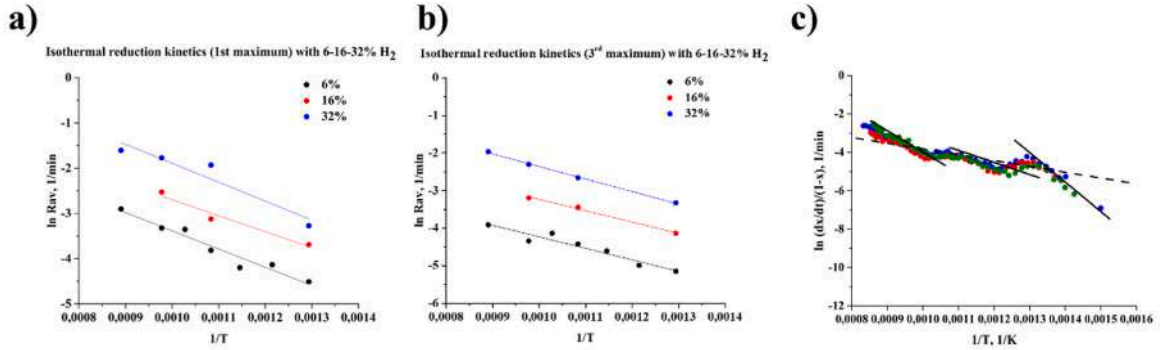

Fig. 10. a) Arrhenius plots from isothermal reduction tests at different temperature and H_2 concentration for the first peak; b) Arrhenius plots from isothermal reduction tests at different temperature and H_2 concentration for the third peak c) Arrhenius plots from non-isothermal reduction tests at different heating rates (2–10 °C/min).

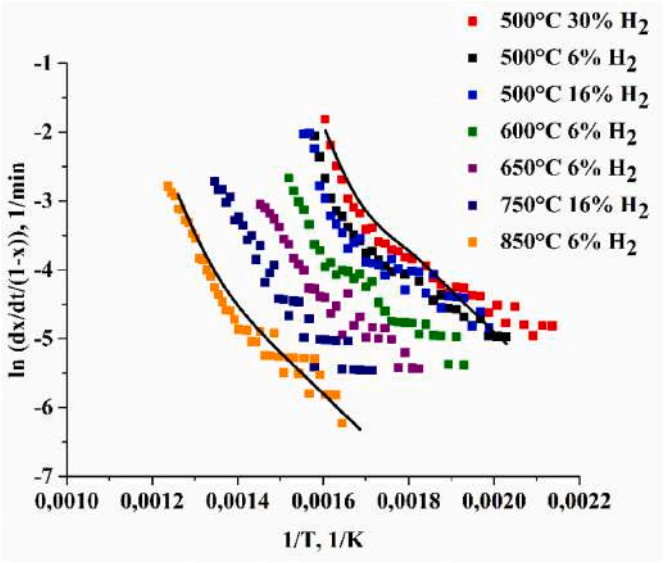

Fig. 12. Arrhenius plots of re-oxidation after different pre-reduction steps.

Table 7
Re-oxidation kinetics.

Reduction pre-treatment		Kinetic parameters	
T,°C	H_2	E_1	E_2
		30 kJ/mol	70 kJ/mol
		k_1	k_2
		1/min	1/min
500	6%	9.0E+02	2.2E+09
500	16%	6.7E+02	1.5E+09
500	32%	1.2E+03	4.0E+09
600	6%	4.0E+02	6.5E+08
650	6%	2.2E+02	2.2E+08
750	16%	1.2E+02	5.9E+07
850	6%	4.5E+01	8.9E+06

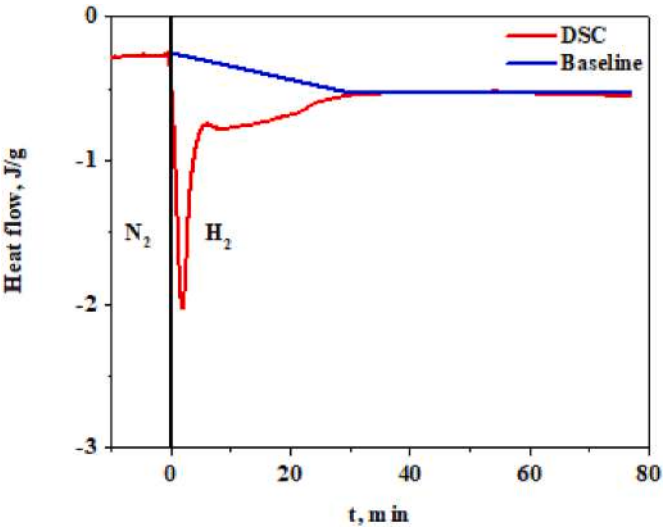

Fig. 13. Pattern of DSC curves during isothermal reduction.

Where p_g is the reactant gas concentration and x the conversion degree.

Of course, more complex kinetic models could have been selected; however, the present work does not aim to develop the best possible kinetic model for iron ore reduction ever, but rather to reconcile the scattered results obtained by different research groups using simple first power laws expressions.

Examples of the Arrhenius plots obtained from both I-TGA and NI-TGA are reported in Fig. 10, in which solid lines represent kinetic regressions.

It can be observed, that in the isotherm Arrhenius plot a single linearity range is obtained whose slope corresponds to an activation energy in the order of 30 kJ/mol. On the contrary, in NI-Arrhenius plots, when curves obtained at different heating rates are plotted in the same graph, three linearity regions can be clearly identified, at T < 500 °C, at T = 550–700 °C and at T > 700 °C. Kinetic parameters for each of these three stages can be obtained from regression over each linear range and are reported in Table 6. In this case, the remarkably higher values of 133 and 83 kJ/mol are found for T < 500° and T > 700 °C. These values are in good agreement with those obtained in Ref. [40] using a NI approach. A lower activation value, in the order of 30 kJ/mol and comparable with that calculated from isothermal tests, both in the present work and in other papers [7,44,46], is instead obtained in the intermediate temperature range.

In Fig. 11, the Arrhenius plots from I-TGA are compared with the Arrhenius plots of NI- tests. It can be observed, that the data points of the isothermal tests fall on the Arrhenius plots of the NI-TGA tests, but due to more limited number of points, the existence of multiple linearity regions cannot be appreciated and could lead to a wrong "overall" kinetic expression with lower values of the activation energy. This is consistent with results from the literature, where generally low values of activation energies are reported from isothermal TG campaigns [49,50]. Noteworthy, the same wrong estimates of kinetic parameters would be obtained if the Arrhenius plots of the NI-TG tests were also fitted by a single line.

Altogether, the best way to obtain kinetic parameters of iron ore reduction seems by regression analysis over the three linear ranges, which become clear when Arrhenius plots of NI-TGA tests performed at different heating rates are overlaid, Fig. 10c.

The set of kinetic parameters obtained accordingly, is reported in Table 6.

A similar approach has been followed for kinetic analysis of oxidation tests. The Arrhenius plots for the NI-oxidation tests have been reported in Fig. 12. In this case, two linearity ranges can be identified. Both are clearly affected by the severity of the proceeding reduction step. The pre-exponential factors obtained for re-oxidation in the two linearity ranges of the Arrhenius plot for samples that have undergone reduction pre-treatments under different conditions are reported in Table 7.

The most reactive sample is the one reduced at 500 °C with 32% H_2. The least reactive the one reduced at 850 °C with 6% H_2. Notably, the value of the pre-exponential factor, having fixed the activation energy at 30 kJ/mol, decreases by two orders of magnitude when the temperature of the pre-reduction increases from 500 °C to 850 °C. This means that the sample reduced at 500 °C with 32% H_2 is more reactive than the one reduced at 850 °C with 6% H_2 by two orders of magnitude.

5. Heat of reaction

The integral of the DSC curves (after baseline subtraction) provides an estimate of the reaction heat *per* mass of IOK sample, Fig. 13.

DSC curves obtained during isothermal TGA-DSC tests exhibit a pattern composed of a sharp peak followed by a second slight one. The results obtained for the different isothermal reaction tests (at T = 500–750 °C) provide an average value of $\triangle H = 0.9$ kJ/g. Furthermore, for the re-oxidation test the same procedure was adopted, which provides values of $\triangle H = -9.6$ kJ/g.

6. Conclusions

The present work reports the results of an experimental campaign of reduction with hydrogen and re-oxidation with air of natural Iron Ore

with relatively low content of impurities and small particle size, in the absence of gas diffusion limitations.

1. It is shown that results of the parameters of the kinetic rate expressions can be affected by the choice of a non-isothermal or an isothermal kinetic analysis approach, in close relation to the fact that the reduction path changes across the threshold temperature of 550°C–600 °C, switching from two to three stages of reaction. To avoid mistakes and remove common artifacts and assess the kinetics of each three-reaction stages, non-isothermal kinetic methods are recommended over isothermal ones.
2. An annealing type effect is observed upon reduction-oxidation steps. In particular, the rate of oxidation can decrease by up to two orders of magnitude after severe pre-reduction steps. Accordingly, the reaction conditions must be carefully selected, and an "annealing" type effect should be taken into account in advanced kinetic models.
3. Upon reiterated reduction and oxidation steps, reactivity changes in a non-monotonous way, exhibiting a minimum in reduction propensity after 3 cycles. The observation is relevant for the design of cyclic operations or looping processes with iron ores.
4. Preliminary results on the changes in crystalline hematite phase over reduction and re-oxidation steps have been obtained. These may be imply spin-flip effects and ultimately changes in ferromagnetic properties of the materials. However, comprehension of the structural changes of the iron ores upon annealing and cyclic operation and their relation with reactivity and properties of the materials certainly deserves further investigation in future work.

CRediT authorship contribution statement

Francesca Cerciello: Writing – original draft, Writing – review & editing, Data curation, Formal analysis, Investigation. **Antonio Fabozzi:** Data curation, Investigation, Writing – original draft, Writing – review & editing. **Christoph Yannakis:** Writing – review & editing. **Sebastian Schmitt:** Funding acquisition, Resources. **Oğuzhan Narin:** Conceptualization, Funding acquisition, Supervision. **Viktor Scherer:** Funding acquisition, Supervision, Writing – review & editing. **Osvalda Senneca:** Conceptualization, Supervision, Writing – original draft, Writing – review & editing.

Declaration of competing interest

The authors declare the following financial interests/personal relationships which may be considered as potential competing interests: Viktor Shereer reports financial support was provided by Deutsche Forschungsgemeinschaft (DFG, German Research Foundation). Antonio Fabozzi reports financial support was provided by European Union - NextGenerationEU. If there are other authors, they declare that they have no known competing financial interests or personal relationships that could have appeared to influence the work reported in this paper.

Acknowledgements

The work was partially funded by the Deutsche Forschungsgemeinschaft (DFG, German Research Foundation) – Project-ID 422037413 – TRR 287 (Teilweise gefördert durch die Deutsche Forschungsgemeinschaft (DFG) – Projektnummer 422037413 – TRR 287).

Antonio Fabozzi acknowledges funding from the European Union - NextGenerationEU under the National Recovery and Resilience Plan (PNRR), Mission 04 Component 2 Investment 3.1, Project "ECCSELLENT - Development of ECCSEL-R.I. ItaLian facilities: usEr access, services and loNg-Term sustainability" Code: IR0000020 - CUP F53C22000560006.

iENTRANCE@ENL - Infrastructure for ENergy TRAnsition aNd Circular Economy @ EuroNanoLab" - Code IR0000027 – CUP B33C22000710006 –European Union - NextGenerationEU under the National Recovery and Resilience Plan (NRRP), Mission 04, Component 2, Investment 3.1.

The authors acknowledge Luciano Cortese for the SEM investigations, Luigi Stanzione and Andrea Capuozzo for XRF analysis, Massimo Urciolo for granulometric analysis.

Appendix A. Supplementary data

Supplementary data to this article can be found online at https://doi.org/10.1016/j.ijhydene.2024.04.008.

References

[1] Taylor KG, Konhauser KO. Iron in earth surface systems: a major player in chemical and biological processes. Elements 2011;7:83–8.
[2] Ashraf M, Khan I, Usman M, Khan A, Shah SS, Khan AZ, et al. Hematite and magnetite nanostructures for green and sustainable energy harnessing and environmental pollution control: a review. Chem Res Toxicol 2019;33:1292–311.
[3] Monazam ER, Breault RW, Siriwardane R. Kinetics of magnetite (Fe3O4) oxidation to hematite (Fe2O3) in air for chemical looping combustion. Ind Eng Chem Res 2014;53:13320–8.
[4] Mendoza EYM, Santos AS, López EV, Drozd V, Durygin A, Chen J, et al. Iron oxides as efficient sorbents for CO2 capture. J Mater Res Technol 2019;8:2944–56.
[5] Chubar N, Gerda V, Szlachta M, Yablokova G. Effect of Fe oxidation state (+ 2 versus+ 3) in precursor on the structure of Fe oxides/carbonates-based composites examined by XPS, FTIR and EXAFS. Solid State Sci 2021;121:106752.
[6] Du W, Yang S, Pan F, Shangguan J, Lu J, Liu S, et al. Hydrogen reduction of hematite ore fines to magnetite ore fines at low temperatures. J Chem 2017;2017.
[7] Kuila SK, Chatterjee R, Ghosh D. Kinetics of hydrogen reduction of magnetite ore fines. Int J Hydrogen Energy 2016;41:9256–66.
[8] Heidari A, Niknahad N, Iljana M, Fabritius T. A review on the kinetics of iron ore reduction by hydrogen. Materials 2021;14:7540.
[9] von Bogdandy L, Engell H-J. The reduction of iron ores: scientific basis and technology. 2013. Springer Science & Business Media.
[10] Pineau A, Kanari N, Gaballah I. Kinetics of reduction of iron oxides by H2: Part I: low temperature reduction of hematite. Thermochim Acta 2006;447:89–100.
[11] Chen H, Zheng Z, Chen Z, Bi XT. Reduction of hematite (Fe2O3) to metallic iron (Fe) by CO in a micro fluidized bed reaction analyzer: a multistep kinetics study. Powder Technol 2017;316:410–20.
[12] Li L, Polanco C, Ghahreman A. Fe (III)/Fe (II) reduction-oxidation mechanism and kinetics studies on pyrite surfaces. J Electroanal Chem 2016;774:66–75.
[13] Buerge IJ, Hug SJ. Kinetics and pH dependence of chromium (VI) reduction by iron (II). Environ Sci Technol 1997;31:1426–32.
[14] Rose AL, Waite TD. Kinetic model for Fe (II) oxidation in seawater in the absence and presence of natural organic matter. Environ Sci Technol 2002;36:433–44.
[15] Guo D, Hu M, Pu C, Xiao B, Hu Z, Liu S, et al. Kinetics and mechanisms of direct reduction of iron ore-biomass composite pellets with hydrogen gas. Int J Hydrogen Energy 2015;40:4733–40.
[16] Jeong MH, Lee DH, Bae JW. Reduction and oxidation kinetics of different phases of iron oxides. Int J Hydrogen Energy 2015;40:2613–20.
[17] Scharm C, Küster F, Laabs M, Huang Q, Volkova O, Reinmöller M, et al. Direct reduction of iron ore pellets by H2 and CO: in-situ investigation of the structural transformation and reduction progression caused by atmosphere and temperature. Miner Eng 2022;180:107459.
[18] Fruehan R, Li Y, Brabie L, Kim EJ. Final stage of reduction of iron ores by hydrogen. Scand J Metall 2005;34:205–12.
[19] Li K, Khanna R, Zhang J, Liu Z, Sahajwalla V, Yang T, et al. The evolution of structural order, microstructure and mineral matter of metallurgical coke in a blast furnace: a review. Fuel 2014;133:194–215.
[20] Ortiz M, Gayán P, De Diego LF, García-Labiano F, Abad A, Pans MA, et al. Hydrogen production with CO2 capture by coupling steam reforming of methane and chemical-looping combustion: use of an iron-based waste product as oxygen carrier burning a PSA tail gas. J Power Sources 2011;196:4370–81.
[21] Matzen M, Pinkerton J, Wang X, Demirel Y. Use of natural ores as oxygen carriers in chemical looping combustion: a review. Int J Greenh Gas Control 2017;65:1–14.
[22] Jeong MH, Sun J, Han GY, Lee DH, Bae JW. Successive reduction-oxidation activity of FeOx/TiO2 for dehydrogenation of ethane and subsequent CO2 activation. Appl Catal B Environ 2020;270:118887.
[23] Bergthorson JM. Recyclable metal fuels for clean and compact zero-carbon power. Prog Energy Combust Sci 2018;68:169–96.
[24] Debiagi P, Rocha RC, Scholtissek A, Janicka J, Hasse C. Iron as a sustainable chemical carrier of renewable energy: analysis of opportunities and challenges for retrofitting coal-fired power plants. Renew Sustain Energy Rev 2022;165:112579.
[25] Jiang X, Wang L, Shen FM. Shaft furnace direct reduction technology-Midrex and Energiron. Adv Mater Res 2013;805:654–9.
[26] Sohn H. Suspension ironmaking technology with greatly reduced energy requirement and CO2 emissions. Steel Times Int 2007;31:68.
[27] Kohse-Höinghaus K, Oßwald P, Cool TA, Kasper T, Hansen N, Qi F, et al. Biofuel combustion chemistry: from ethanol to biodiesel. Angew Chem Int Ed 2010;49:3572–97.
[28] Senneca O, Apicella B, Russo C, Cerciello F, Salatino P, Heuer S, et al. Pyrolysis and thermal annealing of coal and biomass in CO2-rich atmospheres. Energy & Fuels 2018;32:10701–8.

[29] Dhawan N, Manzoor U, Agrawal S. Hydrogen reduction of low-grade banded iron ore. Miner Eng 2022;187:107794.
[30] Hu H, Yuan Y, Lim S, Wang CH. Phase structure dependence of magnetic behaviour in iron oxide nanorods. Mater Des 2020;185:108241.
[31] Takeda M, Onishi T, Nakakubo S, Fujimoto S. Physical properties of iron-oxide scales on Si-containing steels at high temperature. Mater Trans 2009;50:2242–6.
[32] Kim S-H, Zhang X, Ma Y, Souza Filho IR, Schweinar K, Angenendt K, et al. Influence of microstructure and atomic-scale chemistry on the direct reduction of iron ore with hydrogen at 700 C. Acta Mater 2021;212:116933.
[33] Zhang G-C, Luo G-P, Jia P-F, Wang Y-C, Chai Y-F. Effect of basicity on the reduction swelling properties of iron ore briquettes. High Temp Mater Process 2021;40: 193–203.
[34] Kissinger HE. Reaction kinetics in differential thermal analysis. Anal Chem 1957; 29:1702–6.
[35] Friedman HL. Kinetics of thermal degradation of char-forming plastics from thermogravimetry. Application to a phenolic plastic. In: Journal of polymer science part C: polymer symposia: wiley Online Library; 1964. p. 183–95.
[36] Flynn JH, Wall LA. A quick, direct method for the determination of activation energy from thermogravimetric data. J Polym Sci B Polym Lett 1966;4:323–8.
[37] Ozawa T. A new method of analyzing thermogravimetric data. Bull Chem Soc Jpn 1965;38:1881–6.
[38] Burnham AK, Braun RL. Global kinetic analysis of complex materials. Energy & Fuels 1999;13:1–22.
[39] Starink M. A new method for the derivation of activation energies from experiments performed at constant heating rate. Thermochim Acta 1996;288: 97–104.
[40] Munteanu G, Ilieva L, Andreeva D. TPR data regarding the effect of sulfur on the reducibility of α-Fe2O3. Thermochim Acta 1999;329:157–62.
[41] Munteanu G, Ilieva L, Andreeva D. Kinetic parameters obtained from TPR data for α-Fe2O3 and Auα-Fe2O3 systems. Thermochim Acta 1997;291:171–7.
[42] Lin H-Y, Chen Y-W, Li C. The mechanism of reduction of iron oxide by hydrogen. Thermochim Acta 2003;400:61–7.
[43] Jozwiak W, Kaczmarek E, Maniecki T, Ignaczak W, Maniukiewicz W. Reduction behavior of iron oxides in hydrogen and carbon monoxide atmospheres. Appl Catal Gen 2007;326:17–27.
[44] Sastri M, Viswanath R, Viswanathan B. Studies on the reduction of iron oxide with hydrogen. Int J Hydrogen Energy 1982;7:951–5.
[45] Abd Elhamid M, Khader M, Mahgoub A, El Anadouli B, Ateya B. Autocatalytic reduction of hematite with hydrogen under conditions of surface control: a vacancy-based mechanism. J Solid State Chem 1996;123:249–54.
[46] Barde AA, Klausner JF, Mei R. Solid state reaction kinetics of iron oxide reduction using hydrogen as a reducing agent. Int J Hydrogen Energy 2016;41:10103–19.
[47] Lee G-Y, Choi J-P, Song J-I, Jung S-S, Lee J-S. The kinetics of isothermal hydrogen reduction of nanocrystalline Fe2O3 powder. Mater Trans 2014;55:1611–7.
[48] Kuila SK, Chaudhuri S, Chatterjee R, Ghosh D. Reduction of magnetite ore fines with hydrogen. Proceedings of 4th international conference on chemical engineering dhaka: chemical engineering department, BUET2014.p. 81..
[49] Grigiante M, Brighenti M, Antolini D. Analysis of the impact of TG data sets on activation energy (E a) Case study applied to torrefaction of biomasses by means of isoconversional methods. J Therm Anal Calorim 2017;129:553–65.
[50] Fabozzi A, Cerciello F, Senneca O. Reduction of Iron Oxides for CO2 Capture Materials. Energies 2024;17(7):1673.